Inorganic Chemistry

Article

pubs.acs.org/IC

Heteroleptic Complexes of Cyclometalated Platinum with Triarylformazanate Ligands

Evanta Kabir, Chia-Hua Wu, Judy I-Chia Wu, and Thomas S. Teets*

Department of Chemistry, University of Houston, 3585 Cullen Boulevard Room 112, Houston, Texas 77204-5003, United States

Supporting Information

ABSTRACT: Formazanates are a ligand class featuring a 1,2,4,5-tetraazapentadienyl core, with variable substitution at the 1, 3, and 5 positions. Here we describe a set of four heteroleptic cylcometalated platinum complexes containing triarylformazanate ligands. The complexes are prepared by metathesis reactions of chloro-bridged dimers [Pt(C∧N)(μ-Cl)]2 (C∧N = 2-phenylpyridine or 2-(2,4-difluorophenyl)-pyridine) with triarylformazans in the presence of base. X-ray diffraction studies reveal the molecular structures of three such complexes. Cyclic voltammograms and UV−vis absorption spectra of the complexes show features characteristic of both the cyclometalated platinum fragment and the formazanate, with the latter giving rise to two reversible one-electron reductions in the CV and an intense visible $\pi \rightarrow \pi^*$ absorption which is red-shifted by >100 nm relative to the free formazan. The electronic structures and redox properties of the complexes were further investigated by UV−vis spectroelectrochemistry and density functional theory calculations. All of the experimental and theoretical work points to a frontier molecular orbital manifold where the formazanate π and π^* orbitals are substantially mixed with d-orbitals derived from the platinum center.

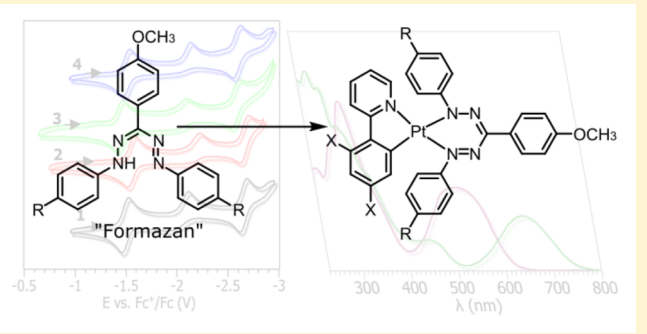

INTRODUCTION

Formazans have been known for over a century, with most of the early work on these compounds devoted to synthetic procedures, structural elucidation, and evaluation of their biomedical applications.[1] Featuring a 1,2,4,5-tetraazapentadienyl core, the chelating ability of these compounds has long been recognized, with sporadic accounts of their transition-metal coordination chemistry appearing over the past several decades.[2−7] The desirable optical properties of formazans, namely, intense visible absorption, coupled with their accessible reduction potentials, make them attractive ligands for a number of applications, and in recent years, the coordination chemistry of formazans has experienced a renaissance. The latest accounts have expanded the chemistry of formazans with first-row transition metals[8] and palladium,[9] demonstrated their utility as supporting ligands for copper-mediated oxygen activation,[10,11] and paired formazans with other redox-active ligands in heteroleptic cobalt complexes.[12] Furthermore, zinc complexes of formazanates have been used to showcase their redox noninnocence,[13,14] and luminescent boron chelates have emerged which further expound the redox and optical properties of these compounds.[15−19]

In spite of these numerous previous accounts, there are only sparse examples of formazan ligands coordinated to third-row transition metals. There are a number of third-row transition metal complexes of dithizonates, which contain a formazan-like core, but in these examples, coordination of the sulfur is proposed, leaving one uncoordinated nitrogen atom.[20] Several articles detail the coordination chemistry of formazanate derivatives with mercury(II); these previous examples all report formazanates with additional *o*-phenoxy or *o*-benzoate groups which are also coordinated.[21,22] The only examples of platinum formazanate complexes likewise consist of *o*-phenoxy-substituted ligands which result in dianionic formazanates coordinated in a tridentate fashion.[23,24] These previous studies described a number of spectroscopic and reactivity properties of the complexes, but the electrochemical properties and electronic structures of these platinum complexes were not elaborated. A partnership between formazans and heavy transition metals offers the possibility of designing complexes where the intense visible absorption and redox activity of formazans are coupled with unique bond activation chemistry and/or triplet excited-state processes engendered by the metal center, motivating further work on such compounds.

Here we describe examples of complexes of platinum(II) with triarylformazan ligands and provide insight into their electronic structures. Reasoning that C∧N cyclometalated ligands would provide a robust and tunable platform to support platinum formazanate complexes, we have prepared heteroleptic bis-chelated complexes with both a formazanate and a C∧N cyclometalated ligand. Furthermore, this approach permits electronic tuning of both the C∧N ligand and formazanate as a means of gauging the extent of electronic communication

Received: November 10, 2015

DOI: 10.1021/acs.inorgchem.5b02595
Inorg. Chem. XXXX, XXX, XXX−XXX

between the platinum center and the formazanate π system. A general synthetic procedure is described for four such complexes, three of which are structurally characterized by single-crystal X-ray diffraction. The electronic structures were interrogated experimentally using cyclic voltammetry, electronic absorption spectroscopy, and UV−vis-NIR spectroelectrochemistry. Whereas formazanate-based reductions are observed, the potentials do shift upon fluorination of the phenylpyridine ligand, consistent with orbital mixing between the platinum center and the formazanate ligand, a contention that is supported by DFT calculations. The optical absorption spectra, with features attributable to both the formazanate and the Pt−C∧N fragment, also evince mixing between the formazanate π orbitals and platinum-centered atomic orbitals. Solvent-dependent electronic absorption spectra reveal some charge-transfer character in the HOMO → LUMO transition, which is confirmed by TD-DFT analysis. All told, this work introduces a new class of robust coordination complexes and demonstrates how binding the formazanate to cyclometalated platinum perturbs the formazanate's electronic structure and gives rise to pronounced changes in the electrochemical and optical properties.

RESULTS

Synthesis of Complexes. Scheme 1 depicts the general synthetic procedure for preparing platinum formazanate complexes **1**−**4**. Two different cyclometalating ligands, 2-phenylpyridine (ppy) and 2-(2,4-difluorophenyl)pyridine (F_2ppy), are combined with two different triarylformazan ligands ($Fz^{Me,OMe}$ and $Fz^{OMe,OMe}$) to furnish a set of four complexes. Reactions in refluxing methanol, with Na_2CO_3 acting as a base, gave good isolated yields (70−94%) of all complexes. ^{1}H, ^{13}C{^{1}H}, and ^{19}F (for **3** and **4**) NMR (Figures S1−S12), in concert with elemental analysis, establish bulk purity and are consistent with the proposed structures.

Scheme 1. Synthesis of Platinum Complexes 1−4

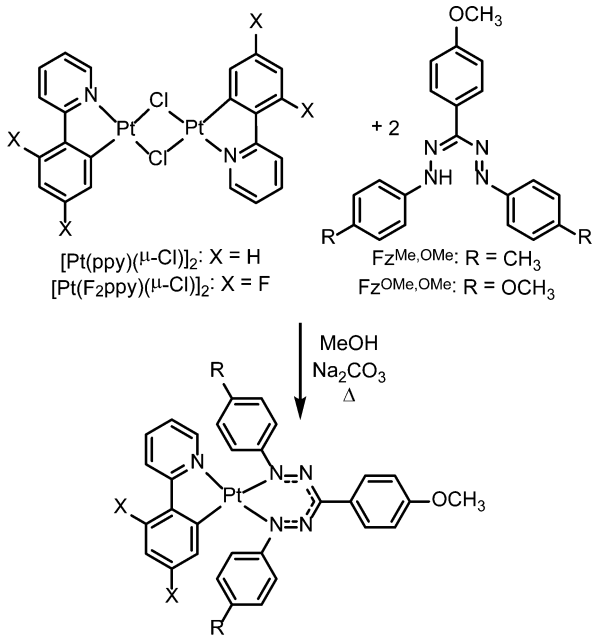

Complexes **1**−**3** were characterized by single crystal X-ray diffraction, with the structures depicted in Figure 1. A summary of crystallographic data for **1**−**3** (Table S1) appears in the Supporting Information. Relevant bond lengths and angles are provided in Table 1. The coordination environments of all complexes are planar, as anticipated for Pt(II); in each case, the Pt atom deviates <0.075 Å from the mean plane of the ligating atoms, and the sum of the bond angles about the Pt center is exactly 360° within experimental error. Bond angles of 80(±2)° are enforced by the six-membered C∧N and formazanate chelates, such that the geometries are not rigorously square planar. The Pt−N bond lengths to the formazanate are in the same range as the distance between the platinum and the pyridyl nitrogen, and they do not appear to depend systematically on the peripheral substitution of the formazanate ligand. A side view of the crystal structures, shown in Figure 2 for complex **3** (**1** and **2** shown in Figures S13 and S14), reveals a "dragonfly" geometry for the formazanate ligand, whereby the three noncoordinated atoms of the formazanate core and the N-aryl substituents are canted out of the coordination plane in opposite directions. A similar coordination mode for formazans has been observed in other transition metal[4,8,12] or BF_2^+[16,17] chelates.

Electrochemistry. Cyclic voltammograms of complexes **1**−**4** are shown in Figure 3. Table 2 summarizes the electrochemical and optical properties of **1**−**4**. The first reduction wave is assigned to a formazanate-based reduction; the nearly equal peak current values and the ca. 60 mV separation between the cathodic and anodic peak potentials are consistent with a reversible one-electron process. The $E_{1/2}$ values are similar for the four complexes. Referenced to ferrocene, this first $E_{1/2}$ value is −1.49 V for complex **1**. Replacing the *para* methyl groups at the 1- and 5-positions of the formazanate with methoxy groups induces a small cathodic shift in the reduction potential, which is observed to be −1.55 V in **2**. This shift is identical in magnitude for **3** ($E_{1/2}$ = −1.44 V) and **4** ($E_{1/2}$ = −1.50 V), and we note that fluorination of the phenylpyridine ligand induces a 50 mV anodic shift, as determined by comparing the potentials for complexes **1** and **3** and those of **2** and **4**.

Two additional reductive waves are observed, an irreversible wave ranging between −2.09 and −2.23 V and another reversible feature between −2.57 and −2.66 V. The potentials of these waves also shift cathodically when $Fz^{Me,OMe}$ is replaced with $Fz^{OMe,OMe}$, with the third reduction wave showing only minimal sensitivity to the formazanate's substitution pattern, shifting by only 10−20 mV when the flanking methyl groups are substituted with methoxy groups.

Complexes **1**−**4** are also oxidized at mild potentials, although in acetonitrile, the oxidation waves in the CVs are complex and typically irreversible (Figure S15). The oxidation waves become reversible in dichloromethane, as shown in Figure S16, suggesting that the irreversibility in acetonitrile results from solvent binding to the oxidized species. Measured in CH_2Cl_2 vs Fc^+/Fc, the first oxidation wave occurs at 0.14 V for **1**, 0.04 for **2**, 0.21 V for **3**, and 0.10 V for **4**, again depending on both the substitution of the formazan and the ppy ligand. A second reversible oxidation is observed in complexes **2**−**4**, occurring at 0.70 V in **2**, 0.89 V in **3**, and 0.66 V in **4**. In complex **1**, this second oxidation is chemically irreversible, with an anodic peak potential of 0.90 V and two return waves observed.

Electronic Absorption and Emission Spectra. Electronic absorption spectra of complexes **1**−**4** were recorded and

DOI: 10.1021/acs.inorgchem.5b02595
Inorg. Chem. XXXX, XXX, XXX−XXX

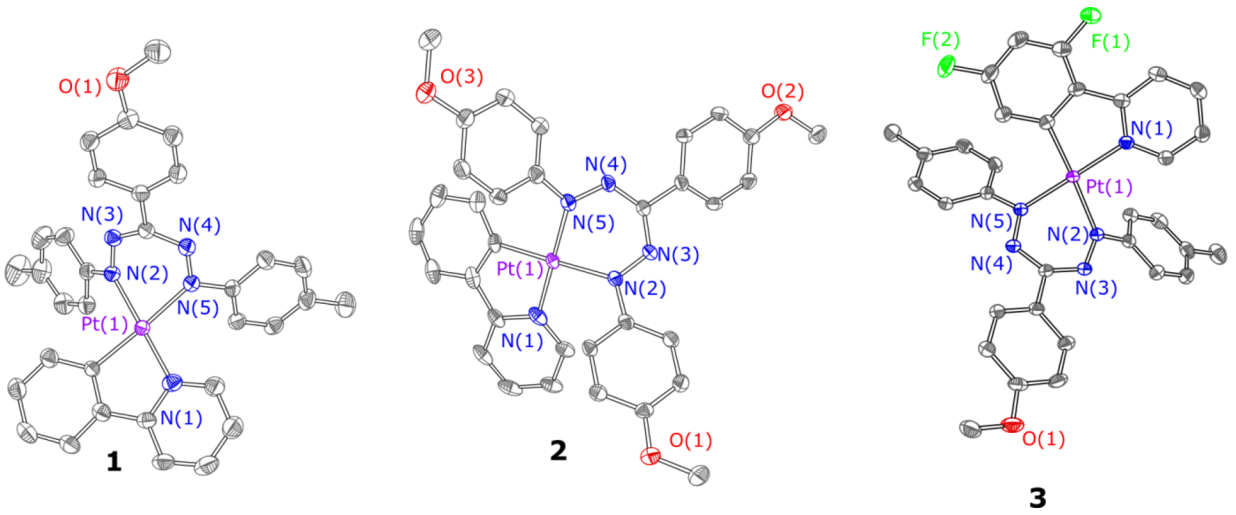

Figure 1. X-ray crystal structures of complexes **1**–**3**. For complex 1, only one crystallographically independent molecule is depicted, and for all structures, hydrogen atoms and solvate molecules are omitted. Data was collected at 213(2) K (**1**) or 123(2) K (**2** and **3**).

Table 1. Summary of Crystallographic Bond Lengths and Angles for Complexes 1–3

	1[a]	2	3
d(Pt–N) (Å) (formazanate, *trans* to N)	2.041(4) 2.055(4)	2.021(4)	2.003(2)
d(Pt–N) (Å) (formazanate, *trans* to C)	2.065(4) 2.059(4)	2.058(3)	2.084(2)
d(Pt–N) (Å) (C∧N)	2.022(4) 2.055(4)	2.020(4)	2.036(2)
d(Pt–C) (Å) (C∧N)	2.006(4) 2.011(4)	2.015(4)	1.998(3)
∠N–Pt–N (deg) (formazanate)	78.67(16) 78.30(15)	80.84(14)	78.92(9)
∠N–Pt–C (deg) (C∧N)	80.14(19) 80.30(19)	80.60(17)	80.31(10)
Σ bond angles (deg)	359.9(7) 359.8(7)	360.0(6)	359.7(4)

[a]Two crystallographically independent molecules.

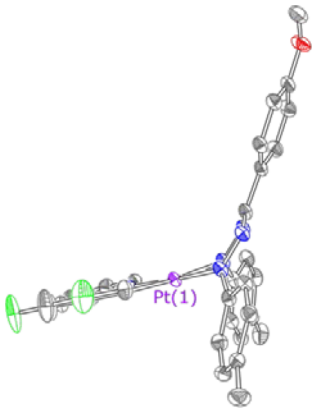

Figure 2. Side view of the crystal structure of complex **3**.

compared to the free formazan ligands. Figure 4 shows the absorption spectra of **1**–**4**, overlaid with their respective free formazan ligand. The data is summarized in Table 2. The broad, intense visible absorption bands in $Fz^{Me,OMe}$ and $Fz^{OMe,OMe}$ occur at 524 nm (ε = 15 000 M^{-1} cm^{-1}) and 545 nm (ε = 14 000 M^{-1} cm^{-1}), respectively. A substantial red shift in this visible

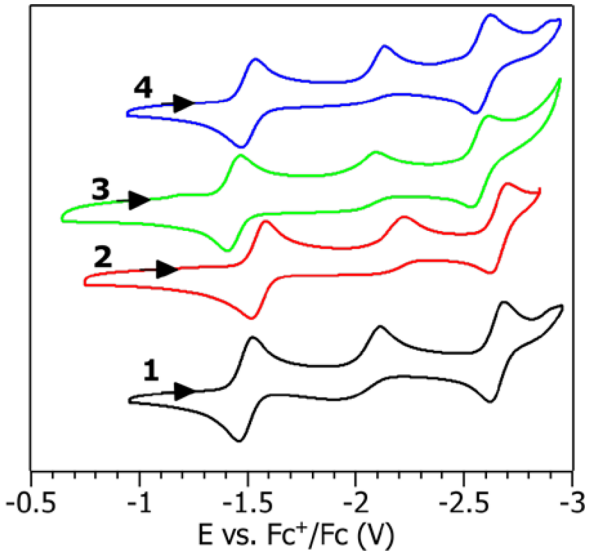

Figure 3. Cyclic voltammograms of complexes **1**–**4**, showing the reduction waves. CVs were recorded in acetonitrile with 0.1 M NBu_4PF_6 supporting electrolyte, using a glassy carbon working electrode and a scan rate of 0.1 V/s. The arrows indicate the scan direction. Currents are normalized to bring the individual traces onto the same scale.

Table 2. Summary of Electrochemical Data and Electronic Absorption Spectra for 1–4[a]

	1	2	3	4
$E_{1/2}$ (V vs Fc^+/Fc)	−1.49, −2.12[b] −2.65	−1.55 −2.23[b] −2.66	−1.44 −2.09[b] −2.57	−1.50 −2.14[b] −2.59
abs. in CH_2Cl_2 λ, nm ($\varepsilon/10^3$)	252 (39) 280 (41) 339[c] (22) 444 (7.9) 664 (12)	256 (36) 277 (33) 353 (18) 449[c] (4.9) 665 (8.3)	251 (35) 269 (32) 294 (25) 338[c] (17) 449 (5.5) 653 (9.6)	254 (43) 292[c] (27) 353 (21) 462 (5.5) 662 (11)

[a]CVs recorded in MeCN solution. [b]Irreversible. [c]Shoulder.

absorption is noted in platinum complexes **1**–**4**, with little dependence of λ_{max} on the formazanate's substituents and molar

DOI: 10.1021/acs.inorgchem.5b02595
Inorg. Chem. XXXX, XXX, XXX–XXX

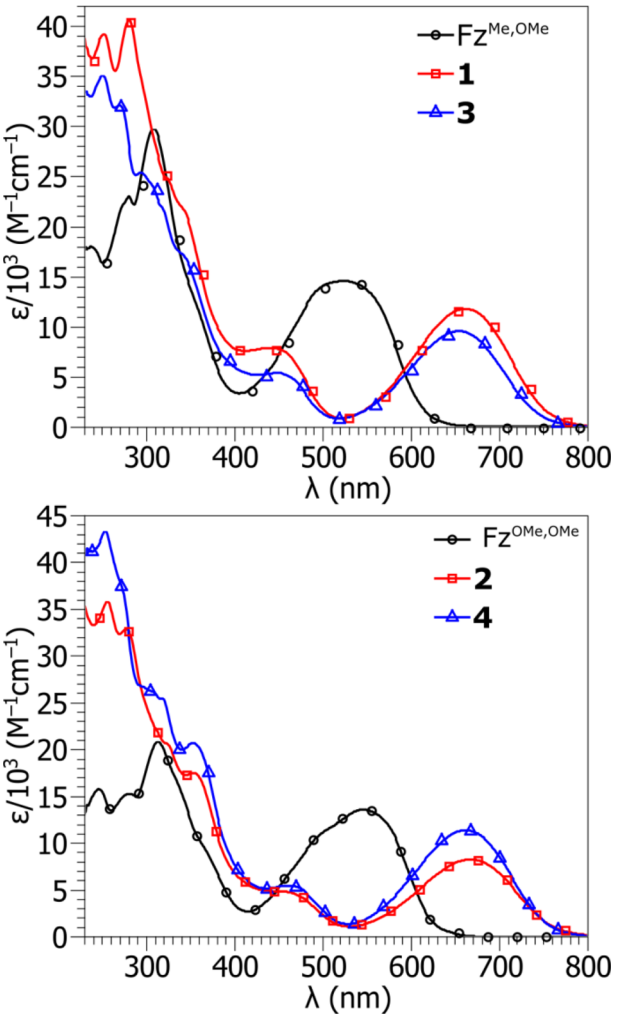

Figure 4. Electronic absorption spectra of **1**–**4**, overlaid with their respective free formazan ligand. Spectra were recorded in dichloromethane solution at room temperature.

absorptivities that are ~10^4 in each case. Complexes **1** and **3**, ligated by $Fz^{Me,OMe}$, show visible absorption bands at 664 (ε = 12 000 M^{-1} cm^{-1}) and 653 nm (ε = 9600 M^{-1} cm^{-1}), respectively, which are only minimally different in $Fz^{OMe,OMe}$ complexes **2** (665 nm, ε = 8300 M^{-1} cm^{-1}) and **4** (662 nm, ε = 11 000 M^{-1} cm^{-1}). This low-energy band shows some sensitivity to solvent polarity, as judged by comparing the absorption spectra recorded in toluene, dichloromethane, and methanol (Figures S17–S20, Table S2). The band shifts to shorter wavelengths as the solvent polarity is increased, but the difference in absorption maxima is <10 nm when comparing toluene solutions to methanol solutions.

In addition to these broad, intense absorption features in the red, complexes **1**–**4** all show a band between 440–460 nm (ε ~ 5000–8000), which is absent in the free formazanate ligand. This absorption band is much more sensitive to the solvent environment than the low-energy band, also shifting to higher energy as the solvent polarity is increased. As a representative example, this band for complex **1** is observed at 460 nm in toluene, 444 nm in dichloromethane, and 413 nm in methanol. Complexes **1**–**4** are nonemissive in the visible region at room temperature and 77 K.

Spectroelectrochemistry. To further investigate the nature of the electrochemical features, we investigated the one- and two-electron reduction chemistry by UV–vis spectroelectrochemistry. For complex **1**, electrolysis at −1.8 V vs Fc^+/Fc, which elicits the first reduction event, gave rise to the spectral changes shown in the top panel of Figure 5. The band at 440 nm was minimally

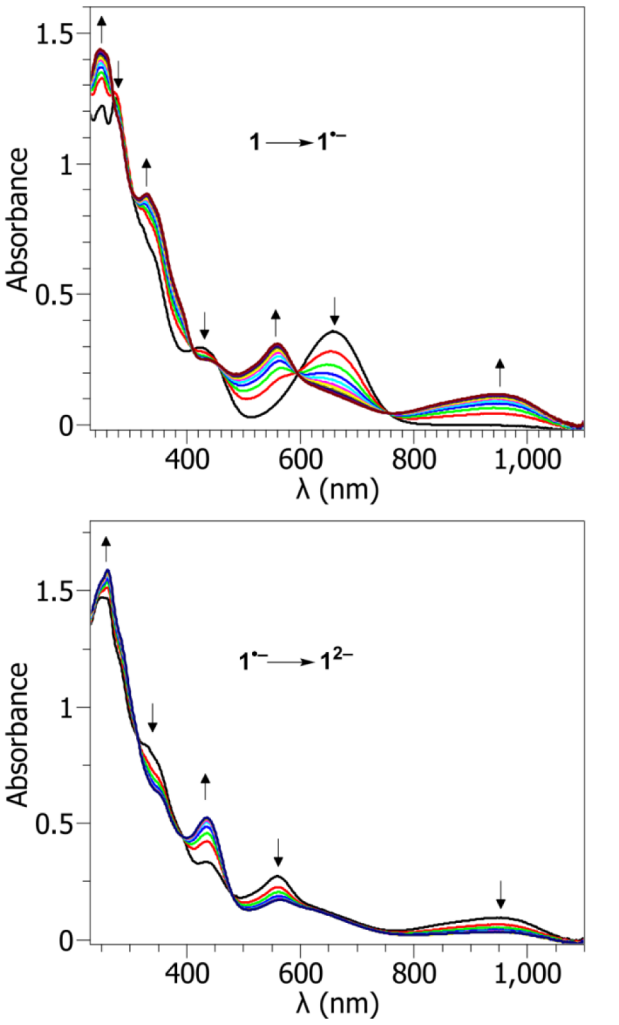

Figure 5. UV–vis-NIR spectroelectrochemistry of complex **1** in MeCN with 0.1 M NBu_4PF_6. The applied potential (vs Fc^+/Fc) was −1.8 V for the first reduction and −2.3 V for the second reduction.

affected by reduction. The low-energy absorption band, occurring at 657 nm in this solvent (acetonitrile), disappears, and new bands at 559 and 950 nm grow in. Reduction of complex **1** at −2.3 V vs Fc^+/Fc induces a second reduction of the complex. This second reduction results in less substantial spectral changes, depicted in the bottom panel of Figure 5. The low-energy transitions attributed to $\mathbf{1}^{\bullet-}$ diminish slightly in intensity during the second reduction, whereas the band that occurs at 425 nm in **1** shifts to 435 nm and intensifies significantly in the two-electron reduced complex $\mathbf{1}^{2-}$. Spectroelectrochemistry was also performed on complex **4**, as shown in Figure S21, with a nearly identical outcome to that of complex **1**.

DFT Computations. DFT-optimized geometries are good matches for the crystal structures, and the "dragonfly" shape of the formazanate is reproduced. Time-dependent density functional theory (TD-DFT) computations characterized the key electronic transitions of two 1,3,5-triphenylformazanate ($Fz^{H,H}$) models: an unfluorinated complex **5** Pt(ppy) ($Fz^{H,H}$) and a fluorinated derivative **6** Pt(F_2ppy) ($Fz^{H,H}$). Figure S22 shows the

DOI: 10.1021/acs.inorgchem.5b02595
Inorg. Chem. XXXX, XXX, XXX–XXX

simulated absorption spectra generated from the TD-DFT results. A HOMO → LUMO transition dominates the one-electron, low-energy excitation of both **5** (86% weight) and **6** (87% weight), and the computed wavelengths (**5**: 677 nm, **6**: 658 nm) agree well with the experimental optical spectra of **4** (cf. Table 2). This HOMO → LUMO transition is best described as a formazanate-centered $\pi \rightarrow \pi^*$ excitation with some Pt charge transfer character mixed in. As shown in Figure 6, the HOMO and LUMO orbitals of **5** show substantial mixing of the platinum orbitals with the formazanate π-system. Population analyses show that the HOMO for both **5** and **6** exhibit a ca. 15% contribution from the Pt-centered orbitals (primarily d_{z^2}), while the LUMO displays only ca. 2% Pt character. Direct comparisons of the molecular electrostatic potential (MEP) maps of **5** and **6** (see Figure 7) reveal that fluorination modestly reduces the electrostatic potential of the Pt center (**5**: V(Pt) = −399.12 V, **6**: V(Pt) = −398.93 V) as well as the nitrogen atoms at the 2- (**5**: V(N2) = −499.69 V, **6**: V(N2) = −499.53 V) and 4- (**5**: V(N4) = −499.61 V, **6**: V(N4) = −499.54 V) positions of the 1,2,4,5-tetraazapentadienyl core.

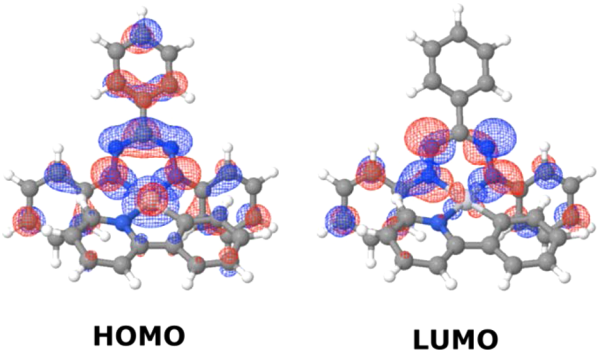

Figure 6. Computed HOMO and LUMO contour plots for the model complex (**5**) Pt(ppy) ($Fz^{H,H}$) (contour level = 0.3 au).

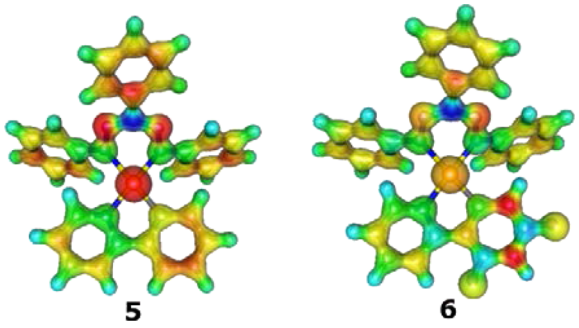

Figure 7. Computed MEP plots for the model complexes, (**5**) Pt(ppy) ($Fz^{H,H}$) and (**6**) Pt(F_2ppy) ($Fz^{H,H}$), employing the Molekel program (isosurface values were set to 0.1 for illustrative purposes).

DISCUSSION

The coordination chemistry of formazanate ligands with third-row transition metals remains underexplored, and in particular, the electrochemical and optical properties of such complexes have received little attention. Seeking a versatile platform to support platinum formazanate coordination compounds, this initial work explored the design and synthesis of heteroleptic complexes, where the formazanate is partnered with a C∧N cyclometalated phenylpyridine derivative. Our early efforts involved formazan ligands $Fz^{Me,OMe}$ and $Fz^{OMe,OMe}$, where the methyl and methoxy groups provide convenient NMR handles and allow us to probe the effect of electron-donating groups on the electronic properties of the complexes. The synthetic route described in Scheme 1 proved to be general for the four complexes we describe here, and we envision it will be applicable to a wide range of C∧N and formazanate ligands with diverse electronic structures. Once prepared, complexes **1**−**4** have proven to be stable under ambient conditions and can be stored and handled on the benchtop with no evidence for decomposition over a period of several months.

Three of the new complexes were structurally characterized by single-crystal X-ray diffraction. There is a slight asymmetry in the Pt−N bond distances to the chelated formazanate; the distances trans to the phenyl are longer, consistent with a stronger trans influence of phenyl as compared to pyridine. Also of note, the Pt−N bond distances involving the C∧N ligand and the formazanate are quite similar; on average the former are only marginally shorter than the latter. The Pt−N (C∧N) bond distances observed here, which average 2.033(4) Å for the three complexes, are considerably longer than the corresponding distance in Pt(ppy) (acac) (1.979(6) Å).[25] That said, the bond distances we observe here between the platinum and the C∧N ligand are markedly similar to those reported for cyclometalated platinum complexes with 5-aryldipyrrinato ligands.[26] Although there is some variability among the complexes reported here, the average Pt−N and Pt−C distance for **1**−**3** are within 0.01 Å of the corresponding distances in the dipyrrinato complexes. In addition, the average formazanate Pt−N distances we observe are quite similar to the pyrrinato Pt−N distances in these previously reported complexes,[26] which represent rare examples of cyclometalated platinum with monoanionic diaza ligands. There are few literature compounds which are directly comparable to the complexes we describe here, but we do not believe that the structural metrics observed **1**−**3** are remarkable in any way.

Complexes **1**−**4** are dark green in color, owing to a low-energy transition centered at ∼660 nm with $\varepsilon \sim 10^4$ M^{-1} cm^{-1}. We assign this transition as a formazanate-centered $\pi-\pi^*$ transition, which is significantly perturbed from that of the free ligand, which has a low energy λ_{max} of 520−540 nm. Consistent with this assignment, this low-energy band shows minimal dependence on solvent polarity, decreasing by no more than 10 nm when the solvent is changed from toluene to methanol, with dichloromethane solutions giving maxima between these extremes. Calculations confirm the nature of this transition. TD-DFT reveals an intense low-energy transition which is principally HOMO→LUMO, consisting mostly of formazanate $\pi \rightarrow \pi^*$ character. The calculations also reveal some Pt(d)→ formazanate charge transfer character in the excited state, consistent with the slight solvent dependence of the this absorption maximum. The perturbation of the formazanate's $\pi \rightarrow \pi^*$ absorption in these platinum complexes is larger than that observed in boron[17,19] or zinc[14] formazanate complexes, though in group 10 Ni(II)[8] complexes, similarly large bathochromic shifts are observed. The participation of Pt atomic orbitals in the frontier molecular orbitals is responsible for the large perturbation of the HOMO→LUMO gap when the formazanate is coordinated to platinum. A second absorption band is observed at higher energy, consistent with a Pt(d)→C∧N(π^*) MLCT transition, as seen in other cyclometalated platinum complexes.[27] The solvent dependence of this absorption band clearly points to substantial charge transfer character, with the absorption maximum shifting by ∼30

DOI: 10.1021/acs.inorgchem.5b02595
Inorg. Chem. XXXX, XXX, XXX−XXX

nm or more when the solvent is changed from toluene to methanol.

The electrochemical behavior of complexes **1**−**4** offers additional insight into their electronic structure. Although the potential of the first reversible process depends on both the formazanate and the C∧N ligand, we assign it primarily to a formazanate-based reduction. Related Pt(II) cyclometalates, supported by redox-inactive acac ligands, are reduced at much more negative potentials, −2.41 V for Pt(ppy) (acac), and −2.29 V for Pt(F_2ppy) (acac).[27] Our observed potentials of ca. −1.5 V are much more in line with the ligand-based reductions observed in other triarylformazanate complexes. Several boron formazanates have been electrochemically characterized, and a BF_2^+ chelate of $Fz^{Me,OMe}$ shows a first reduction potential of −0.90 V.[17] Metal complexes of triarylformazans are rarer and tend to be more difficult to reduce; a series of homoleptic zinc triarylformazanates are reduced at potentials in the range of −1.2 to −1.8 V,[14] similar to the values we observe for Pt(II) complexes **1**−**4**. Moreover, DFT calculations on model complexes Pt(ppy) ($Fz^{H,H}$) (**5**) and Pt(F_2ppy) ($Fz^{H,H}$) (**6**) reveal LUMOs that are almost exclusively localized on the formazanate ligand, also suggesting the formazanate as the site of the first reduction event. The assignment of the first reduction wave is further supported by UV−vis spectroelectrochemistry. Reduction of **1** by one electron results in the disappearance of the low-energy HOMO→LUMO band (657 nm in MeCN) and the growth of two new low-energy bands, one at 559 nm and one at 950 nm. These new features are entirely consistent with a one-electron reduced formazanate and are qualitatively similar to the absorption bands in other compounds featuring formazanate-derived radical ligands. As described previously, one-electron reduction of zinc[28] and boron[15,29] formazanate complexes gives rise to two new absorption bands, which resemble the absorption bands of verdazyl radicals. The two new bands flank the $\pi\rightarrow\pi^*$ band of the closed-shell, monoanionic formazanate,[13] with one growing at higher energy, and one appearing at lower energy. The absorption bands we observe for $\mathbf{1}^{\bullet-}$ and $\mathbf{4}^{\bullet-}$, which contain a one-electron reduced verdazyl-type ligand, are substantially red-shifted from those of zinc or boron formazanates and verdazyl radicals, much in the same manner as the HOMO→LUMO absorption in neutral **1**−**4** undergoes a significant red-shift upon coordination to platinum.

The behavior of the first formazanate-based reduction provides further evidence for the mixing of platinum- and formazanate-centered orbitals in the frontier MO's. Addition of electron-donating methoxy groups to the formazanate predictably perturbs the reduction potential to a more negative value; replacing *p*-CH_3 groups on the 1- and 5-aryl substituents with *p*-OCH_3 induces a 60 mV cathodic shift in this potential. By replacing ppy (complexes **1** and **2**) with F_2ppy (**3** and **4**), the first reduction wave is *anodically* shifted by 50 mV. This is consistent with an electronic structure where the Pt is donating electron density to the redox-active formazanate. The electron donation is attenuated by fluorination of the phenylpyridine ligand, which results in a positive shift in the formazanate-based reduction potential. This supposition is supported by computational studies of the model complexes. The molecular electrostatic potential map shows that the addition of electronegative fluorine substituents to the ppy ligand pulls electron density from the opposing formazanate, which is consistent with the observation that the F_2ppy complexes are easier to reduce by 50 mV, even though the reduction event is primarily localized on the formazanate.

Two subsequent reduction waves are observed in complexes **1**−**4**, and these are likewise sensitive to electronic modification of both the formazanate and C∧N ligand. The first of these, which is irreversible, is assigned to a Pt−C∧N based reduction, and the most cathodically shifted reversible reduction is assigned to a second formazanate-based reduction. The assignment of these waves is supported by literature precedent. The two reversible waves are separated by ca. 1.1 V, which is similar to the separation between the successive reduction potentials of boron formazanates,[17,19] leading us to favor an assignment of the wave at ca. −2.6 V to a second formazanate-based reduction. Furthermore, this second formazanate-based wave is considerably less sensitive to addition of a methoxy group to the 1- and 5-aryl positions, which is also true for previously studied boron chelates when making analogous substitutions. The spectroelectrochemistry for the second reduction is inconclusive but is consistent with the assignment of the wave as a platinum-centered reduction. With this reduction (Figure 5, bottom), only the Pt(d)→ppy MLCT transition is substantially perturbed, whereas the bands assigned the formazanate(2−) ligand diminish in intensity with no new low-energy features emerging. This suggests that the second electron enters an orbital that is primarily Pt−C∧N-centered and does not further reduce the formazanate. Ultimately, a more definitive assignment of the second and third reduction waves will come from investigation of a larger suite of complexes, with more electronically diverse C∧N and formazanate ligands, which are expected to perturb the reduction potentials more substantially and will clarify the assignment of these features.

CONCLUSION

In this work, we outlined a general synthetic strategy for coordinating formazanate ligands to cyclometalated platinum complexes. The desirable properties of the formazanate, namely, the facile ligand-based redox chemistry and intense visible absorption, are retained in these complexes, and these features motivate an extension to other transition metals and supporting ligand platforms where differential mingling of metal-based and formazanate-based orbitals could lead to unique properties. Efforts are underway to prepare an expanded library of complexes with more structurally and electronically diverse C∧N and formazanate ligands, with the goal of gaining a more thorough understanding of the electronic structure and ensuant properties of this novel class of complexes.

EXPERIMENTAL SECTION

Materials. Reactions were carried out in a nitrogen atmosphere using standard Schlenk techniques. Solvents, starting materials, and reagents were of commercial origin and used without further purification, unless stated otherwise below. Dichloromethane and toluene for UV−vis spectroscopy and acetonitrile for electrochemical measurements were dried by the method of Grubbs,[30] passing through dual alumina columns on a commercial solvent purification system (SPS). The acetonitrile was further dried by storage over 3A molecular sieves. Tetrabutylammonium hexafluorophosphate ($TBAPF_6$) was recrystallized from hot ethanol and ferrocene was sublimed at ambient pressure before use in electrochemical experiments. $CDCl_3$ for NMR spectroscopy was stored over potassium carbonate and molecular sieves to remove acidic impurities and moisture. The ligand 3-*p*-methoxyphenyl-1,5-di-*p*-tolylformazan ($Fz^{Me,OMe}$) was prepared by the method of Hicks et al.[28] The ligand 1,3,5-tri-*p*-methoxyphenylformazan ($Fz^{OMe,OMe}$) was prepared by the same method; details of its synthesis have not been previously reported and are given below. The platinum precursors $[Pt(ppy)(\mu\text{-}Cl)]_2$ (ppy =2-phenylpyridine) and [Pt(F_2ppy)-

DOI: 10.1021/acs.inorgchem.5b02595
Inorg. Chem. XXXX, XXX, XXX−XXX

(μ-Cl)]$_2$ (F_2ppy =2-(2,4-difluorophenyl)pyridine) were prepared as previously described, using conventional heating and a 1:1 mol ratio of K_2PtCl_4 and the C∧N ligand.[31] (*Note*: Many other references describe the syntheses of these dimers, using >2 equiv of C∧N with K_2PtCl_4. We have found, as reported in the referenced synthetic procedure, that using excess C∧N ligand leads to the formation of substantial amounts of monomeric Pt(κ_2-C∧N)(κ_1−N-C∧N) (Cl) as a side product.)

Physical Methods. NMR spectra were recorded at room temperature using a JEOL ECA-600 NMR spectrometer. UV−vis absorption spectra were recorded in CH_2Cl_2 solutions in screw-capped quartz cuvettes using an Agilent Cary 60 UV−vis spectrophotometer. Cyclic voltammetry (CV) measurements were performed with a CH Instruments 602E potentiostat interfaced with a nitrogen glovebox via wire feedthroughs. Samples were dissolved in acetonitrile with 0.1 M $TBAPF_6$ as a supporting electrolyte. A 3 mm diameter glassy carbon working electrode, a platinum wire counter electrode, and a silver wire pseudoreference electrode were used. Potentials were referenced to an internal standard of ferrocene. Spectroelectrochemistry measurements were executed in thin-layer quartz cuvettes, using a patterned "honeycomb" electrode from Pine Research Instrumentation consisting of a gold working electrode and a platinum counter electrode, in combination with a separate silver wire pseudoreference. Solutions were thoroughly sparged with argon prior to measurement, and spectra were recorded on a Cary 8354 diode array spectrophotometer. IR spectra were recorded on solid samples using a Nicolet iS10 Spectrometer with an ATR (attenuated total reflectance) accessory. Elemental analyses were performed by Midwest Microlab, LLC.

Computational Details. Geometry optimizations and time-dependent density functional theory (TD-DFT) computations for **5** and **6** were performed at the B97/Def2-TZVPP level employing Gaussian09. For TD-DFT, only the lowest-energy excited state was computed at the B97/Def2-TZVPP level, whereas the full simulated spectrum shown in Figure S22 was computed at B97D/Def2-SVPP//B97D/Def2-TZVPP. Molecular electrostatic potential (MEP) maps were computed at B97/Def2-SVPP//B97/Def2-TZVPP and plotted with the Molekel program. The optimized geometries of both **5** and **6** exhibit a characteristic "dragonfly" shape (see Cartesian coordinates included in the Supporting Information) and match well with the crystal structures of **1**−**4**. TD-DFT computations quantified the HOMO → LUMO transition oscillator strengths and composition of the one-electron excitation transitions.

Preparation of $Fz^{OMe,OMe}$. 4-Methoxyphenylhydrazine hydrochloride (5.76g, 33.0 mmol) was combined with triethylamine (8.34 mL, 59.7 mmol) and ethanol (50 mL). After the mixture was stirred for 30 min, 4-methoxybenzaldehyde (4.01 mL, 33.0 mmol) was added, and the mixture was allowed to stir for an additional 2 h, at which time a dark orange precipitate had formed. The reaction mixture was treated with sodium carbonate hydrate (11.87 g, 111.5 mmol), tetrabutyl ammonium bromide (1.07 g, 3.34 mmol), water (100 mL) and dichloromethane (100 mL) and stirred at 0 °C for another 1 h. A solution of a diazonium salt made from stirring 4-methoxy aniline (4.68 g, 38.0 mmol), sodium nitrite (3.17 g, 46.6 mmol), water (10 mL), and hydrochloric acid (10 mL) for 1 h at 0 °C was then added dropwise to the hydrazone mixture. After addition, the organic phase in the biphasic reaction turned blood red. After stirring for 2 h at room temperature, the organic layer was collected and washed with water (500 mL) in a separatory funnel. The aqueous layer was extracted with an additional 20 mL of dichloromethane. $MgSO_4$ (5 g) was added to the combined organic layer to remove the extra water, and the solution was taken to dryness on a rotary evaporator after filtration. The solid was dissolved in boiling methanol followed by cooling to furnish a dark purple microcrystalline solid. Yield: 6.20 g (48.2%). ^{1}H NMR (400 MHz, $CDCl_3$) δ: 15.38 (br, s, 1H, NH), 8.05 (m, 2H, ArH), 7.62 (m, 4H, ArH), 6.95−6.99 (m, 6H, ArH), 3.870 (s, 3H, OCH_3), 3.867 (s, 6H, OCH_3).

*Pt(ppy) ($Fz^{Me,OMe}$) (**1**).* [Pt(ppy)(μ-Cl)]$_2$ (100 mg, 0.130 mmol), $Fz^{Me,OMe}$ (93 mg, 0.26 mmol) and sodium carbonate hydrate (110 mg, 1.04 mmol) were combined in MeOH (12 mL), and the mixture was deoxygenated by bubbling with nitrogen. The mixture was refluxed at 65 °C, and a color change was observed from deep purple to bright green over the course of refluxing for 16 h. Reaction completion was confirmed by TLC. The methanol was removed via rotary evaporation, and the product was taken up in dichloromethane. The mixture was filtered through a short silica column, eluting with dichloromethane until all of the green color had passed through. The solution was taken to dryness in vacuo. A spectroscopically pure green microcrystalline solid was obtained by adding pentane to a concentrated THF solution. Yield 133.6 mg (70%). Material satisfactory for elemental analysis required recrystallization from CH_2Cl_2/pentane. The crystalline material was spectroscopically and electrochemically indistinguishable from the initially isolated powder. ^{1}H NMR (400 MHz, $CDCl_3$) δ: 8.19 (d, J = 8.7 Hz, 2H, ArH), 8.14 (d, J = 8.2 Hz, 3H, ArH), 8.00 (d, J = 6.8 Hz, 2H, ArH), 7.58−7.67 (m, 2H, ArH), 7.43 (d, J = 6.8 Hz, 1H, ArH), 7.15 (d, J = 8.4 Hz, 2H, ArH), 7.10 (d, J = 8.0 Hz, 2H, ArH), 6.93−6.99 (m, 3H, ArH), 6.80 (t, J = 7.2 Hz, 1H, ArH), 6.72 (d, J = 6.8 Hz, 1H, ArH), 6.68 (t, J = 6.8 Hz, 1H, ArH), 3.87 (s, 3H, OCH_3), 2.38 (s, 6H, CH_3). ^{13}C{^{1}H} NMR: δ 168.5, 159.9, 153.8, 151.1, 150.9, 150.6, 148.0, 145.9, 138.4, 136.86, 136.84, 136.6, 130.1,129.8, 129.2, 129.1, 126.4, 125.8, 124.7, 123.6, 123.0, 121.0, 118.5, 113.7, 55.5, 21.3, 21.2. IR (solid): 3020 (m), 2951 (m), 2924 (m), 2908 (m), 2831 (m), 1607 (s), 1584 (m), 1510 (s), 1494 (s), 1482 (s), 1439 (m), 1427 (m), 1389 (m) cm^{-1}. Anal. Calcd for $C_{33}H_{29}N_5OPt$: C, 56.09; H, 4.14, N, 9.91. Found: C, 56.32, H, 4.41, N, 9.63.

*Pt(ppy) ($Fz^{OMe,OMe}$) (**2**).* The title compound was prepared by the general method described above for complex **1**, using 100 mg of [Pt(ppy)(μ-Cl)]$_2$ and 101 mg of $Fz^{OMe,OMe}$. Yield: 189 mg (94.0%). ^{1}H NMR (400 MHz, $CDCl_3$) δ: 8.14−8.25 (m, 5H, ArH), 7.96−8.00 (m, 2H, ArH), 7.58−7.67 (m, 2H, ArH), 7.43 (d, J = 7.6 Hz, 1H, ArH), 6.79−6.98 (m, 8H, ArH), 6.66−6.74 (m, 2H, ArH), 3.87 (s, 3H, OCH_3), 3.84 (s, 3H, OCH_3), 3.83 (s, 3H, OCH_3). ^{13}C{^{1}H} NMR: 168.6, 159.9, 158.6, 158.4, 153.8, 151.0, 148.1, 147.1, 146.5, 146.0, 138.5, 136.9, 132.4, 130.3, 129.4, 127.0, 126.4, 125.9, 123.7, 123.0, 121.2, 118.6, 114.5, 113.7, 55.79, 55.76, 55.6. Anal. Calcd for $C_{33}H_{29}N_5O_3Pt$: C, 53.66; H, 3.96, N, 9.48. IR (solid): 3045 (m), 3000 (m), 2951 (m), 2928 (m), 2907 (m), 2834 (m), 1597 (s), 1582 (s), 1509 (s), 1495 (s), 1483 (s), 1459 (s), 1438 (s) cm^{-1}. Anal. Calcd for $C_{33}H_{29}N_5O_3Pt$: C, 53.66; H, 3.96, N, 9.48. Found: C, 53.68, H, 3.91, N, 9.39.

*Pt(F_2ppy) ($Fz^{Me,OMe}$) (**3**).* The title compound was prepared by the general method described above, using 100 mg of [Pt(F_2ppy)(μ-Cl)]$_2$ and 85 mg of $Fz^{Me,OMe}$. Yield: 151 mg (85.7%). Recrystallization from CH_2Cl_2/pentane gave the product as **3**·0.5CH_2Cl_2, evident from ^{1}H NMR spectra of the crystals and combustion analysis data. ^{1}H NMR (400 MHz, $CDCl_3$) δ: 8.15−8.19 (m, 3H, ArH), 8.06 (d, J = 8.2 Hz, 2H, ArH), 7.96−8.01 (m, 3H, ArH), 7.69 (t, J = 7.8 Hz, 1H, ArH), 7.11−7.16 (m, 4H, ArH), 6.97−7.01 (m, 2H, ArH), 6.66−6.69 (m, 1H, ArH), 6.37−6.43 (m, 1H, ArH), 6.20 (dd, J = 9.6, 2.4 Hz, 1H, ArH), 3.87 (s, 3H, OCH_3), 2.40 (s, 3H, CH_3), 2.38 (s, 3H, CH_3). ^{13}C{^{1}H} NMR: 165.1 (d, J_{CF} = 7.4 Hz), 162.1 (dd, J_{CF} = 343, 12 Hz), 160.4 (dd, J_{CF} = 346, 12 Hz), 160.0, 153.9, 152.8 (d, J_{CF} = 5.9 Hz), 151.0, 150.4, 150.2, 138.9, 137.3, 136.8, 129.9, 129.7, 129.6, 129.2, 126.4, 125.7, 124.7, 122.2 (d, J_{CF} = 21 Hz), 120.9, 118.7 (d, J_{CF} = 16 Hz), 113.8, 99.6 (t, J_{CF} = 27 Hz), 55.5, 21.24, 21.21. IR (solid): 3077 (m), 3023 (m), 3004 (m), 2950 (m), 2922 (m), 2855 (m), 2838 (m), 1601 (s), 1571 (s), 1560 (s), 1513 (s), 1497 (s), 1480 (s), 1427 (s), 1407 (s) cm^{-1}. Anal. Calcd for $C_{33}H_{27}F_2N_5OPt$·0.5CH_2Cl_2: C, 51.25; H, 3.59, N, 8.92. Found: C, 51.44, H, 3.55, N, 8.58.

*Pt(F_2ppy) ($Fz^{OMe,OMe}$) (**4**).* The title compound was prepared by the general method above, using 100 mg of [Pt(F_2ppy)(μ-Cl)]$_2$ and 93 mg of $Fz^{OMe,OMe}$. Yield: 148 mg (80.4%). ^{1}H NMR (400 MHz, $CDCl_3$) δ: 8.19−8.22 (m, 3H, ArH), 8.14 (d, J = 9.2 Hz, 2H, ArH), 7.97−7.99 (m, 3H, ArH), 7.66−7.70 (m, 1H, ArH), 6.97−7.00 (m, 2H, ArH), 6.85−6.91 (m, 4H, ArH), 6.68−6.72 (m, 1H, ArH), 6.38−6.44 (m, 1H, ArH), 6.23 (dd, J = 9.2, 2.2 Hz, 1H, ArH), 3.87 (s, 3H, OCH_3), 3.83 (s, 6H, OCH_3). ^{13}C{^{1}H} NMR: 165.2 (d, J_{CF} = 5.9 Hz), 162.2 (dd, J_{CF} = 347, 13 Hz), 160.5 (dd, J_{CF} = 352, 12 Hz), 160.0, 158.9, 158.5, 153.8, 152.9 (d, J_{CF} = 5.9 Hz), 150.9, 146.3, 146.1, 139.0, 129.8, 129.6, 126.9, 126.4, 125.8, 122.3 (d, J_{CF} = 19 Hz), 121.0, 118.7 (d, J_{CF} = 18 Hz), 114.5, 113.83, 113.75, 99.6 (t, J_{CF} = 27 Hz), 55.74, 55.71, 55.5. IR (solid): 3070(m), 3043 (m), 3006 (m), 2938 (m), 2911 (m), 2836 (m), 1598 (s), 1574 (s), 1514 (s), 1494 (s), 1481 (s), 1464 (s), 1451 (s), 1434 (s),

DOI: 10.1021/acs.inorgchem.5b02595
Inorg. Chem. XXXX, XXX, XXX−XXX

1405 (s) cm^{-1}. Anal. Calcd for $C_{33}H_{27}F_2N_5O_3Pt$: C, 51.16; H, 3.51, N, 9.04. Found: C, 50.98, H, 3.53, N, 8.90.

X-ray Crystallography Details. Single crystals of **1**−**3** were grown by layering concentrated CH_2Cl_2 solutions with pentane. Crystals were mounted on a Bruker Apex II three-circle diffractometer using Mo Kα radiation (λ = 0.71073 Å). The data was collected at 213(2) K (**1**) or 123(2) K (**2** and **3**) and was processed and refined within the APEXII software. Structures were solved by direct methods in SHELXS and refined by standard difference Fourier techniques in the program SHELXL. Hydrogen atoms were placed in calculated positions using the standard riding model and refined isotropically; all non-hydrogen atoms were refined anisotropically. The structure of **3** contained a heavily disordered solvent molecule, likely dichlormethane, which was removed using the SQUEEZE function within Platon. The crystal of **1** was found to be partially desolvated; one dichloromethane was modeled as half-occupied, and a second was modeled as a two-part disorder about a special position with total one-half occupancy. Distance restraints (SADI) were used for all 1,2 and 1,3 distances within the disordered solvent molecules, and rigid bond restraints SIMU and DELU were employed for the thermal displacement parameters. Crystallographic details are summarized in Table S1.

■ ASSOCIATED CONTENT

Supporting Information

The Supporting Information is available free of charge on the ACS Publications website at DOI: 10.1021/acs.inorgchem.5b02595.

Crystallographic data tables, NMR spectra for new compounds, alternative views of the crystal structures of **1** and **2**, additional cyclic voltammograms, solvent-dependent electronic absorption spectra, UV−vis-NIR spectroelectrochemistry of complex **4**, simulated absorption spectra for **5** and **6**, and optimized Cartesian coordinates for **5** and **6** (PDF)

X-ray data (CIF)

■ AUTHOR INFORMATION

Corresponding Author

*E-mail: tteets@uh.edu.

Author Contributions

The manuscript was written through contributions of all authors. All authors have given approval to the final version of the manuscript.

Notes

The authors declare no competing financial interest.

■ ACKNOWLEDGMENTS

This work was supported by the University of Houston and by a grant from the Welch Foundation (Grant No. E-1887). We thank Prof. Loi Do for allowing use of the UV−vis spectrophotometer, and Prof. Karl Kadish and Dr. Yuanyuan Fang for helpful discussions regarding spectroelectrochemistry.

■ REFERENCES

(1) Nineham, A. W. *Chem. Rev.* **1955**, *55*, 355−483.
(2) Hunter, L.; Roberts, C. B. *J. Chem. Soc.* **1941**, 823−826.
(3) Irving, H.; Gill, J. B.; Cross, W. R. *J. Chem. Soc.* **1960**, 2087−2095.
(4) Dale, D. *J. Chem. Soc. A* **1967**, 278−287.
(5) Budesinsky, B.; Svecova, J. *Inorg. Chem.* **1971**, *10*, 313−317.
(6) Siedle, A. R.; Pignolet, L. H. *Inorg. Chem.* **1980**, *19*, 2052−2056.
(7) Kawamura, Y.; Yamauchi, J.; Ohya-Nishiguchi, H. *Bull. Chem. Soc. Jpn.* **1993**, *66*, 3593−3599.
(8) Gilroy, J. B.; Patrick, B. O.; McDonald, R.; Hicks, R. G. *Inorg. Chem.* **2008**, *47*, 1287−1294.
(9) Gilroy, J. B.; Ferguson, M. J.; McDonald, R.; Hicks, R. G. *Inorg. Chim. Acta* **2008**, *361*, 3388−3393.
(10) Hong, S.; Hill, L. M. R.; Gupta, A. K.; Naab, B. D.; Gilroy, J. B.; Hicks, R. G.; Cramer, C. J.; Tolman, W. B. *Inorg. Chem.* **2009**, *48*, 4514−4523.
(11) Hong, S.; Gupta, A. K.; Tolman, W. B. *Inorg. Chem.* **2009**, *48*, 6323−6325.
(12) Protasenko, N. A.; Poddel'sky, A. I.; Bogomyakov, A. S.; Fukin, G. K.; Cherkasov, V. K. *Inorg. Chem.* **2015**, *54*, 6078−6080.
(13) Chang, M.-C.; Dann, T.; Day, D. P.; Lutz, M.; Wildgoose, G. G.; Otten, E. *Angew. Chem., Int. Ed.* **2014**, *53*, 4118−4122.
(14) Chang, M.-C.; Roewen, P.; Travieso-Puente, R.; Lutz, M.; Otten, E. *Inorg. Chem.* **2015**, *54*, 379−388.
(15) Chang, M.-C.; Otten, E. *Chem. Commun.* **2014**, *50*, 7431−7433.
(16) Barbon, S. M.; Reinkeluers, P. A.; Price, J. T.; Staroverov, V. N.; Gilroy, J. B. *Chem. - Eur. J.* **2014**, *20*, 11340−11344.
(17) Barbon, S. M.; Price, J. T.; Reinkeluers, P. A.; Gilroy, J. B. *Inorg. Chem.* **2014**, *53*, 10585−10593.
(18) Hesari, M.; Barbon, S. M.; Staroverov, V. N.; Ding, Z.; Gilroy, J. B. *Chem. Commun.* **2015**, *51*, 3766−3769.
(19) Barbon, S. M.; Staroverov, V. N.; Gilroy, J. B. *J. Org. Chem.* **2015**, *80*, 5226−5235.
(20) Meriwether, L. S.; Breitner, E. C.; Sloan, C. L. *J. Am. Chem. Soc.* **1965**, *87*, 4441−4448.
(21) Petersen, R. L.; McFarland, J. T.; Watters, K. L. *Bioinorg. Chem.* **1978**, *9*, 355−367.
(22) Zhang, H.-Y.; Sun, W.-X.; Wu, Q.-A.; Zhangb, H.-Q.; Chen, Y.-Y. *Synth. React. Inorg. Met.-Org. Chem.* **2000**, *30*, 571−582.
(23) Bait, S.; Meuldijk, J.; Renkema, W. E. *Transition Met. Chem.* **1980**, *5*, 357−361.
(24) Balt, S.; Meuldijk, J. *Inorg. Chim. Acta* **1981**, *47*, 217−223.
(25) Bossi, A.; Rausch, A. F.; Leitl, M. J.; Czerwieniec, R.; Whited, M. T.; Djurovich, P. I.; Yersin, H.; Thompson, M. E. *Inorg. Chem.* **2013**, *52*, 12403−12415.
(26) Bronner, C.; Baudron, S. A.; Hosseini, M. W.; Strassert, C. A.; Guenet, A.; De Cola, L. *Dalton Trans.* **2010**, *39*, 180−184.
(27) Brooks, J.; Babayan, Y.; Lamansky, S.; Djurovich, P. I.; Tsyba, I.; Bau, R.; Thompson, M. E. *Inorg. Chem.* **2002**, *41*, 3055−3066.
(28) Gilroy, J. B.; McKinnon, S. D. J.; Koivisto, B. D.; Hicks, R. G. *Org. Lett.* **2007**, *9*, 4837−4840.
(29) Gilroy, J. B.; Ferguson, M. J.; McDonald, R.; Patrick, B. O.; Hicks, R. G. *Chem. Commun.* **2007**, 126−128.
(30) Pangborn, A. B.; Giardello, M. A.; Grubbs, R. H.; Rosen, R. K.; Timmers, F. J. *Organometallics* **1996**, *15*, 1518−1520.
(31) Godbert, N.; Pugliese, T.; Aiello, I.; Bellusci, A.; Crispini, A.; Ghedini, M. *Eur. J. Inorg. Chem.* **2007**, *2007*, 5105−5111.

DOI: 10.1021/acs.inorgchem.5b02595
Inorg. Chem. XXXX, XXX, XXX−XXX